

Charge-4 Weyl point: Minimum lattice model and chirality-dependent properties

Chaoxi Cui,^{1,2} Xiao-Ping Li,^{1,2} Da-Shuai Ma,^{1,2} Zhi-Ming Yu,^{1,2,*} and Yugui Yao^{1,2}

¹*Centre for Quantum Physics, Key Laboratory of Advanced Optoelectronic Quantum Architecture and Measurement (MOE), School of Physics, Beijing Institute of Technology, Beijing, 100081, China*

²*Beijing Key Lab of Nanophotonics & Ultrafine Optoelectronic Systems, School of Physics, Beijing Institute of Technology, Beijing, 100081, China*

Topological Weyl semimetals have been attracting broad interest. Recently, a new type of Weyl point with topological charge of 4, termed as charge-4 Weyl point (C-4 WP), was proposed in spinless systems. Here, we show the minimum symmetry requirement for C-4 WP is point group T together with \mathcal{T} symmetry or point group O . We establish a minimum tight-binding model for C-4 WP on a cubic lattice with time-reversal symmetry and without spin-orbit coupling effect. This lattice model is a two-band one, containing only one pair of C-4 WPs with opposite chirality around Fermi level. Based on both the low-energy effective Hamiltonian and the minimum lattice model, we investigate the electronic, optical and magnetic properties of C-4 WP. Several chirality-dependent properties are revealed, such as chiral Landau bands, quantized circular photogalvanic effect and quadruple-helicoid surface arc states. Furthermore, we predict that under symmetry breaking, various exotic topological phases can evolve out of C-4 WPs. Our work not only reveals several interesting phenomena associate to C-4 WPs, but also provides a simple and ideal lattice model of C-4 WP, which will be helpful for the subsequent study on C-4 WPs.

I. INTRODUCTION

Since the prediction of Weyl semimetal [1, 2], the search of emergent particles in three-dimensional (3D) crystalline materials has been actively performed [3–7]. These emergent particles can produce many interesting phenomena that can not be found in conventional metals [8–12]. Various emergent particles have been predicted and some of them have been confirmed in experiments [13–28].

Particularly, a complete classification of all the possible emergent particles in 3D systems with time-reversal symmetry (\mathcal{T}) has been recently presented by Yu *et al.* [29], which gives 19 types of spinless particles and 23 types of spinful particles. Among these emergent particles, the two-fold degenerate points, namely, the Weyl points (WPs), always attract the most concern, as they have the simplest models but nontrivial physics.

In Weyl semimetals, the WPs denote isolated doubly degenerate band crossings in the Brillouin zone (BZ), around which the low-energy excitation can be described by the Weyl equation rather than the conventional Schrödinger equation. The conventional WP exhibits linear dispersion along any direction in momentum space and has a topological charge (Chern number) of $\mathcal{C} = \pm 1$. Hence, the conventional WP also is termed as charge-1 WP (C-1 WP) [29]. Due to the nonzero topological charge, the WPs should come in pair with opposite chirality and their projections on boundary are connected by the Fermi arc [1, 4]. Besides, the topological charge can lead to many intriguing electronic, optical and magnetic phenomena [30], which generally have a strong dependence on the sign of the topological charge, e.g. the

chirality. With multiple symmetries, two or three C-1 WPs with same topological charge may merge together, giving rise to the Charge-2 WP (C-2 WP) and Charge-3 Weyl point (C-3 WP) [13, 31]. In contrast to the C-1 WP, the C-2 (C-3) WP features quadratic (cubic) dispersion in a plane and a linear dispersion out-of-plane. Since the band dispersion would affect the shape of Fermi surface and then determines most of the material properties, the C-2 WP and C-3 WP are demonstrated to exhibit signatures distinguished from the C-1 WPs [32–34].

Currently, the exploration of emergent particles is extended to spinless systems, such as phonon spectrum and artificial photonic and phononic crystals [35–42]. The spinless systems are fundamentally different from the spinful systems, reflected in the absence of spin-orbit coupling (SOC) effect. Thus, the time-reversal symmetry \mathcal{T} satisfies $\mathcal{T}^2 = 1$ in spinless systems, while $\mathcal{T}^2 = -1$ in spinful systems. As a consequent, some emergent particles that can not appear in spinful systems would emerge in spinless materials, and vice versa. Recently, a new kind of Weyl point with topological charge of $\mathcal{C} = \pm 4$, e.g. C-4 WP, has been proposed by several independent groups in spinless systems [29, 43, 44], which has a cubic dispersion along (111) direction and quadratic dispersion along any other direction. The C-4 WP was first predicted by Zhang *et. al.* in Ref. [43] (where the C-4 WP is termed as twofold quadruple Weyl node). They found that the C-4 WPs can appear in both the electronic band structure in the absence of SOC effect and the phonon spectra of a series of LaIrSi-type materials. Liu *et al.* [44] also discovered this kind of WP when they systematically studied the symmetry-enforced WP in spinless systems. Yu *et al.* [29], based on the encyclopedia of emergent particles they established, concluded that the C-4 WP is the last two-fold degenerate point in 3D crystals and only appears in spinless systems.

Motivated by the discovery of the new emergent par-

* zhiming-yu@bit.edu.cn

ticle, in this work, we study the minimum symmetry requirement of the C-4 WP, as well as the chirality-dependence of the electronic, optical and magnetic properties. There are two different minimum symmetry conditions that can protect the C-4 WP. One is the point group (PG) O and the other is the PG T together with \mathcal{T} symmetry. We then establish a minimum tight-binding (TB) model of the C-4 WP on a cubic lattice with PG O and \mathcal{T} symmetry. This model has two bands and only one pair of C-4 WPs with opposite topological charge locating at Γ (000) point and R ($\pi\pi\pi$) point, respectively. Four extensive Fermi arcs connecting the projection of the two WPs appear on each boundary of the system. Particularly, the Fermi arcs form unconventional quadruple-helicoid surface states around each WP, and the chirality of the quadruple-helicoid surface states is determined by the chirality of the WP. We also investigate Landau level (LLs) and circular photogalvanic effect (CPGE) of the C-4 WPs, and find that both have a strong dependence on the chirality of the C-4 WP. The chirality-dependent properties of the C-4 WP are further demonstrated by the minimum lattice model. At last, the possible phase transition of C-4 WP under symmetry descend are studied. Our work not only predicts several novel properties of a newly found emergent particle but also establishes a minimum lattice model of the C-4 WP, which would be helpful for the further investigation on this novel particle.

II. CHARGE-4 WEYL POINT

A. Minimum symmetry requirement

In the previous works, all the possible space groups that can protect the C-4 WP have been presented [29, 43, 44]. In this subsection, we study the symmetry protection of the C-4 WP in detail. According to previous studies, one knows that the minimum symmetry requirement for C-4 WP is PG O or the PG T together with \mathcal{T} symmetry.

The generating elements of PG T can be chosen as a three-fold rotation axis along (111) direction ($C_{3,111}^+$), and two orthogonal two-fold rotation axis, such as C_{2x} and C_{2y} . However, the PG T does not have a 2D single-valued irreducible representation (IR) and is not capable to protect a C-4 WP. In the addition of \mathcal{T} symmetry, a pair of conjugated 1D IRs of $C_{3,111}^+$ would be bound together, leading to a 2D corepresentation. The basis state of this 2D corepresentation then can be chose as $\Psi = (|c_3 = e^{i2\pi/3}\rangle, |c_3 = e^{-i2\pi/3}\rangle)$ with c_3 the eigenvalue of $C_{3,111}^+$. Under this basis, the matrix representation of $C_{3,111}^+$ and \mathcal{T} are

$$D(C_{3,111}^+) = \cos \frac{2\pi}{3} \sigma_0 + i \sin \frac{2\pi}{3} \sigma_z, \quad D(\mathcal{T}) = \sigma_x \mathcal{K}, \quad (1)$$

with σ_0 the 2×2 identity matrix, σ_i ($i = x, y, z$) the Pauli matrix and \mathcal{K} the complex conjugate operator. $C_{2x(2y)}$

and $C_{3,111}^+$ satisfy the following algebra

$$C_{2x(2y)}^2 = 1, \quad C_{2x}C_{2y} = C_{2y}C_{2x}, \quad C_{3,111}^+C_{2y} = C_{2x}C_{3,111}^+. \quad (2)$$

Moreover, as $C_{2x(2y)}$ commutes with \mathcal{T} , the matrix representation of $C_{2x(2y)}$ can be expressed as

$$D(C_{2x}) = D(C_{2y}) = \sigma_0. \quad (3)$$

The effective Hamiltonian expanded around the band crossing with this 2D corepresentation is required to be invariant under the symmetry constraints, namely,

$$D(\mathcal{O})H_{k \cdot p}(\mathcal{O}^{-1}\mathbf{k})D^{-1}(\mathcal{O}) = H_{k \cdot p}(\mathbf{k}), \quad (4)$$

where \mathcal{O} runs over the generating elements of PG T and \mathcal{T} . According to the constraint of C_{2x}

$$\sigma_0 H_{k \cdot p}(k_x, -k_y, -k_z) \sigma_0 = H_{k \cdot p}(\mathbf{k}), \quad (5)$$

all the first-order terms in $k_{y(z)}$ must be excluded. Similar analysis applies for C_{2y} , which eliminates the first-order terms in $k_{x(z)}$. Hence, the leading order in $H_{k \cdot p}$ becomes k quadratic. To preserve $C_{3,111}^+$ symmetry, the Hamiltonian along (111) direction must take the form of $H_{k \cdot p}(k_{111}) = f_1(k_{111})\sigma_0 + f_2(k_{111})\sigma_z$ with $f_{1,2}$ an arbitrary function. However, the linear term in $f_{1,2}(k_{111})$ is eliminated by $C_{2x(2y)}$, and the quadratic term in $f_2(k_{111})$ is eliminated by \mathcal{T} , as $\{D(\mathcal{T}), k_{111}^2 \sigma_z\} = 0$. Hence, the effective Hamiltonian, to the leading order, reads

$$\begin{aligned} H_T = & c_1 k^2 \sigma_0 + c_2 k_x k_y k_z \sigma_z \\ & + \sqrt{3} [c_3 (k_x^2 - k_z^2) + c_4 (k_y^2 - k_z^2)] \sigma_x \\ & - [c_3 (k^2 - 3k_y^2) - c_4 (k^2 - 3k_x^2)] \sigma_y, \end{aligned} \quad (6)$$

where $k = \sqrt{k_x^2 + k_y^2 + k_z^2}$ and c 's are real coefficients related to specific materials. This Hamiltonian (6) exhibits cubic band splitting along (111) direction and quadratic splitting for any other directions as shown in Fig. 1, consist with the above analysis. A direct calculation gives that the Chern number for the point is $\mathcal{C} = 4 \times \text{Sign}(c_2)$ [see Fig. 2(d)], indicating the existence of the C-4 WP.

With the addition of $C_{2,110}$ symmetry, the PG T is transformed in O . In contrast to PG T , the PG O alone is enough to produce a C-4 WP. The PG O has only one 2D IR, for which the basis state also can be as $\Psi = (|c_3 = e^{i2\pi/3}\rangle, |c_3 = e^{-i2\pi/3}\rangle)$ with c_3 the eigenvalue of $C_{3,111}^+$. The matrix representation for $C_{2,110}$ under the basis is

$$D(C_{2,110}) = \sigma_x, \quad (7)$$

as $C_{2,110}C_{3,111}^+ = C_{3,111}^-C_{2x}C_{2,110}$. The effective Hamiltonian should be invariant under PG O symmetries, and is obtained as,

$$\begin{aligned} H_O = & c_1 k^2 \sigma_0 + c_2 k_x k_y k_z \sigma_z \\ & + c_3 \left[(k^2 - 3k_z^2) \sigma_x + \sqrt{3} (k_y^2 - k_x^2) \sigma_y \right], \end{aligned} \quad (8)$$

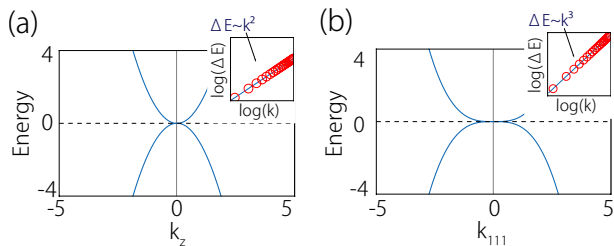


FIG. 1. The band structure of C-4 WP obtained from the Hamiltonian (6) with $c_1 = 0$, $c_2 = 1$, $c_3 = \frac{1}{3}$ and $c_4 = \frac{1}{3}$. (a) and (b) show the energy dispersion along k_z and k_{111} direction. The insets are the log-log plot for the band splitting regarding to the momentum, showing the quadratic (a) and cubic (b) energy dispersion.

which shares same band splitting and topological charge with that of Hamiltonian H_T (6). If we further add \mathcal{T} symmetry to PG O , the effective Hamiltonian for the point would not be changed, as \mathcal{T} commutes with H_O (8) and can not further simplifies Eq. (8).

B. Minimum lattice model

In Ref. [29], a six-band lattice model for the C-4 WP is constructed for the purpose of illustrating the usage of the encyclopedia established there. However, for the study of C-4 WP, a simple lattice model is favored. According to the relationship between site-symmetry of Wyckoff position and the elementary band representation [45, 46], we find the minimum lattice model for C-4 WP is a two-band one.

Consider a cubic lattice belonging to SG 207, which is symmorphic SG with PG O . As illustrated in Fig. 2(a), each unit cell contains an active site locating at $1a$ Wyckoff position. At each site, we put two basis orbitals ($|d_{x^2-y^2}\rangle, |d_{z^2}\rangle$) without spin degree of freedom. Under these basis orbitals, the matrix representation of the generating operators of SG 207 read

$$D(C_{3,111}) = \frac{-\sigma_0 + i\sqrt{3}\sigma_y}{2}, D(C_{2x}) = D(C_{2z}) = \sigma_0, \quad (9)$$

$$D(C_{2,110}) = -\sigma_z, D(\mathcal{T}) = \sigma_0\mathcal{K}. \quad (10)$$

Following the standard approach [47, 48], we construct the required lattice model, which in momentum space may be written as

$$H_{\text{TB}} = t_1(\cos k_x + \cos k_y + \cos k_z) \\ + t_2 \sin k_x \sin k_y \sin k_z \sigma_y + 3t_3(\cos k_x - \cos k_y)\sigma_x \\ - \sqrt{3}t_3(\cos k_x + \cos k_y - 2\cos k_z)\sigma_z, \quad (11)$$

where t_i ($i = 1, 2, 3$) is real model parameters. One can check the lattice model (11) is invariant under the above symmetry operators. Also it is easy to find that the two bands of the model would be degenerate at Γ point and R point, and the effective Hamiltonian expanded around

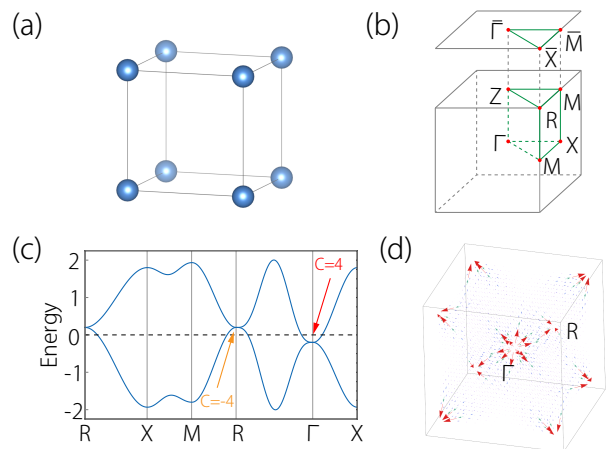


FIG. 2. (a) Crystal structure for the lattice model of C-4 WP. (b) Bulk and surface BZs of the lattice. (c) Band structure of the lattice model (11). (d) Distribution of Berry curvature in the BZ. In the calculation, we set $t_1 = -0.133$, $t_2 = 4$ and $t_3 = 0.539$.

these two points recover the $k \cdot p$ Hamiltonian of C-4 WP (8) but with opposite parameters. Hence, the lattice model contains two C-4 WPs, which respectively locate at Γ point and R point and have opposite chirality.

The calculated band structure of this minimum lattice model (11) is shown in Fig. 2(c), where two C-4 WPs locating at Γ point and R point can be observed. Remarkably, these two WPs are the only two band degeneracies in the model. For comparison, in the lattice model of Weyl semimetal in spinful systems with \mathcal{T} symmetry, the number of the WPs must be at least eight, due to the existence of eight \mathcal{T} -invariant high-symmetry points. The Chern number of the points in Γ point and R point are calculated as $+4$ and -4 , respectively. To further show the topological configuration, we plot the Berry curvature $\mathcal{B}(\mathbf{k})$ for the valence band in Fig. 2(d). The Berry flux emits from the C-4 WP at Γ point and converges onto the C-4 WP at R point, consistent with the Chern number of the two WPs.

III. CHIRALITY-DEPENDENT PROPERTIES

A. Chiral Landau levels

The chiral band degeneracies are expected to exhibit chiral Landau levels (LLs), which can lead to many intriguing phenomena, such as chiral anomaly and negative longitudinal magnetoresistance [49, 50]. Recently, an excellent work by Zhao and Yang [51] proved that the number of the chiral LLs is exactly equal to the topological charge of the degeneracy, solving the long-term speculation about the connection between these two properties. Thus, the C-4 WP would always have four chiral LLs regardless of the direction of magnetic field. In Ref. [29], Yu et. al. numerically calculated the LL spectrum of C-

4 WP when the B -field is along z -direction, and indeed observed four chiral LLs crossing the zero energy.

However, for the systems with C-4 WP, the principal axis is (111)-axis and it is instructive to study the LL spectrum with B -field along (111)-direction. We first rotate the coordinate axis of system and rewrite the effective Hamiltonian of the C-4 WP (8) as

$$\mathcal{H}(\mathbf{q}) = wq^2\sigma_0 - \alpha_1q_z(2q_{\parallel}^2 + q^2 - 3q_z^2)\sigma_3 + \alpha_2 \left[(q_-^2 + 2\sqrt{2}q_zq_+) \sigma_+ + h.c. \right], \quad (12)$$

with $w = c_1$, $\alpha_1 = \frac{c_2}{6\sqrt{3}}$, $\alpha_2 = -c_3$, $q_x = \frac{2k_z - k_x - k_y}{\sqrt{6}}$, $q_y = \frac{k_x - k_y}{\sqrt{2}}$, $q_z = \frac{k_x + k_y + k_z}{\sqrt{3}}$, $q_{\parallel} = \sqrt{q_x^2 + q_y^2 + q_z^2}$, $q_{\pm} = q_x \pm iq_y$ and $\sigma_{\pm} = \frac{1}{2}(\sigma_x \pm i\sigma_y)$. Here, q_z is along the original (111) direction. The Chern number of this model (12) is solely determined by the sign of α_1 , namely $\mathcal{C} = 4 \times \text{Sign}(\alpha_1)$.

Interestingly, one finds that for $q_z = 0$ plane, the Hamiltonian (12) becomes

$$\mathcal{H}(q_z = 0) = wq_{\parallel}^2\sigma_0 + \alpha_2(q_-^2\sigma_+ + h.c.), \quad (13)$$

which exactly is the quadratic Dirac model in bilayer graphene without trigonal warping effect [52]. And for the $q_z \neq 0$ plane, the Hamiltonian (12) becomes a gapped bilayer graphene model with trigonal warping effect, and the strength of the warping effect is proportion to q_z [52].

By applying an external magnetic field along q_z -direction, the electron's motion in q_x - q_y plane is quantized into LLs. We apply the usual Peierls substitution $\mathbf{q} \rightarrow \mathbf{q} + e\mathbf{A}$ in Eq. (12) with \mathbf{A} the vector potential. The LL spectrum of C-4 WP at $q_z = 0$ plane can be easily established as

$$\varepsilon_{n=0}(q_z = 0) = wB, \quad \varepsilon_{n=1}(q_z = 0) = 3wB, \quad (14)$$

for $n = 0, 1$ and

$$\varepsilon_n(q_z = 0) = \left[(2n - 1)w \pm 2\sqrt{w^2 + \alpha_2^2(n - 1)n} \right] B, \quad (15)$$

for $n > 1$. The LL spectrum has a linear dependence on the magnetic field as shown in Fig. 3(c), similar to the conventional electron gas model. Moreover, when $w = 0$, the first two LLs ($n = 0, 1$) would be degenerate at zero energy, and are not sensitive to the field strength. Due to the presence of trigonal warping effect, the analytical expressions of the LL spectrum for $q_z \neq 0$ plane generally can not be obtained. Since the low-energy physics of the LLs, which is relevant for experimental observation, is dominated by the electrons residing at q_x - q_y plane with small q_z , one generally can use the perturbation theory to obtain the low-energy LL spectrum of C-4 WP. We find that the analytic solutions obtained from the first-order perturbation are in good agreement with the numerical results in the low-energy region, as shown in Fig. 3(a-b).

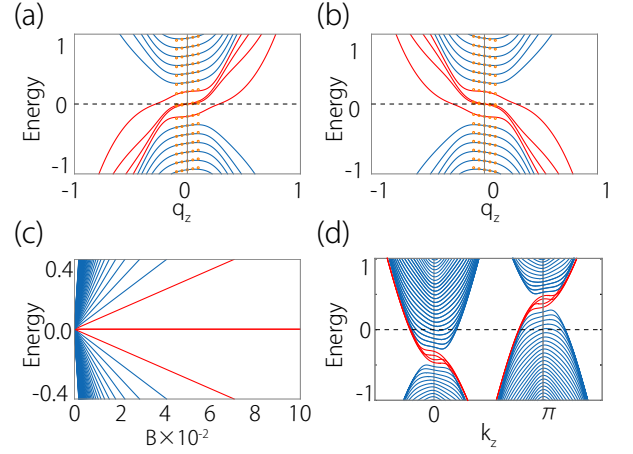


FIG. 3. (a-c) Landau spectrum calculated from the effective model (8) with the B -field along (111)-direction for (a) $w = 0$, $\alpha_1 = -1$ and $\alpha_2 = 2$, and (b) $w = 0$, $\alpha_1 = 1$ and $\alpha_2 = 2$. The orange circles are obtained by first-order perturbation. (c) shows the Landau spectrum as a function of B for $q_z = 0$ plane. (d) Landau spectrum calculated from the lattice model (11) with the B -field along z -direction.

Particularly, four chiral LLs can be clearly observed from the numerical results of the LLs, and one finds that the slope of the four chiral LLs is determined by the sign of α_1 [see Fig. 3(a-b)]. To further demonstrate the chirality-dependent properties of the chiral LLs, we show the numerical result of the Landau spectrum based on the lattice model (11) with the magnetic field along z -direction. Four chiral LLs appear around $k_z = 0$ with negative slope, corresponding to the C-4 WP with $\mathcal{C} = 4$ at Γ point [see Fig. 2(b)]. Meanwhile, another four chiral LLs appear around $k_z = \pi$ with opposite slope, induced by the C-4 WP with $\mathcal{C} = -4$ at R point.

B. Quantized circular photogalvanic effect

Another interesting chirality-dependent phenomena for chiral particle may be the quantized CPGE [53]. The CPGE injection current is defined as

$$\frac{dj_i}{dt} = \beta_{ij}(\omega) [\mathbf{E}(\omega) \times \mathbf{E}^*(\omega)]_j \quad (16)$$

where $\mathbf{E}(\omega) = \mathbf{E}^*(-\omega)$ is the electric field. The CPGE tensor β_{ij} is purely imaginary and can be calculated by

$$\beta_{ij}(\omega) = \frac{\pi e^3}{\hbar V} \epsilon_{jkl} \sum_{\mathbf{k}, n, m} f_{nm}^{\mathbf{k}} \Delta_{\mathbf{k}, nm}^i r_{\mathbf{k}, nm}^k r_{\mathbf{k}, mn}^l \delta(\hbar\omega - \varepsilon_{\mathbf{k}, mn}), \quad (17)$$

with V the sample volume, $\varepsilon_{\mathbf{k}, mn} = \varepsilon_{n, \mathbf{k}} - \varepsilon_{m, \mathbf{k}}$ ($f_{nm}^{\mathbf{k}} = f_n^{\mathbf{k}} - f_m^{\mathbf{k}}$) the energy (Fermi-Dirac distributions) difference between n - and m -the bands, $r_{\mathbf{k}, nm} = i\langle u_n | \partial_{\mathbf{k}} | u_m \rangle$ and $\Delta_{\mathbf{k}, nm}^i = \partial_{k_i} \varepsilon_{\mathbf{k}, nm}$. Juan et al. [53] demonstrated that for WPs, the trace of the CPGE tensor can be quantized

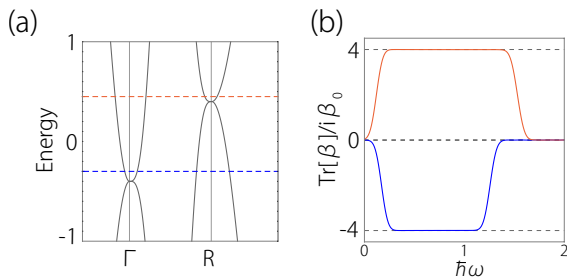


FIG. 4. (a) The band structure of C-4 WP semimetal calculated from the lattice model (11). (b) CPGE traces at different chemical potential ($\mu = -0.3$ and 0.45), denoted as dashed lines in (a).

and its values is proportional to the topological charge \mathcal{C} of WPs,

$$\text{Tr}(\beta) = \sum_{i=x,y,z} \beta_{ii} = -i\beta_0\mathcal{C}, \quad (18)$$

with $\beta_0 = \frac{e^3}{\hbar^2}\pi$. A direct calculation shows the quantized CPGE also applies for the C-4 WP and the quantized value is ± 4 depending on the topological charge of the C-4 WP. Based on the lattice model (11), we numerically calculate the injection current with different Fermi energy, as shown in Fig. 4. Our results show the quantized CPGE indeed can appear in C-4 WP semimetal with suitable Fermi energy and frequency ω . When the CPGE is quantized, the sign of this quantized quantity is determined by the chirality of the C-4 WP, consistent with the theoretical analysis. For example, when the Fermi energy is 0.45 , then only the C-4 WP at R point has contribution to the CPGE effect for $0.1 < \omega < 1.7$. In contrast, when the Fermi energy is set as -0.3 , then only the C-4 WP at Γ point is activated for $0.2 < \omega < 1.4$.

C. Quadruple-helicoid surface states

Topological Weyl semimetals exhibit novel Fermi arc state on the boundary of systems. Remarkably, the Fermi arc state around the projected point of the WP also shows chirality-dependent properties. Since the C-4 WP has a topological charge of $|\mathcal{C}| = 4$, four Fermi arcs would be observed in C-4 WP semimetal. One striking feature of the Fermi arc surface state is that its isoenergy contour is not closed but consist of one or multiple open curves. Fang et al. [54] for the first time pointed out that the surface state of a conventional C-1 WP around the projected point on boundary is equivalent to a helicoid. Later, Zhang et al. [55] showed the surface state of a Dirac point with topological charge of $|\mathcal{C}| = 2$ is a double helicoid. Thus, one can expect the surface state around the projection of a C-4 WP would be a quadruple helicoid, namely, four screw surfaces wind around the C-4 WP.

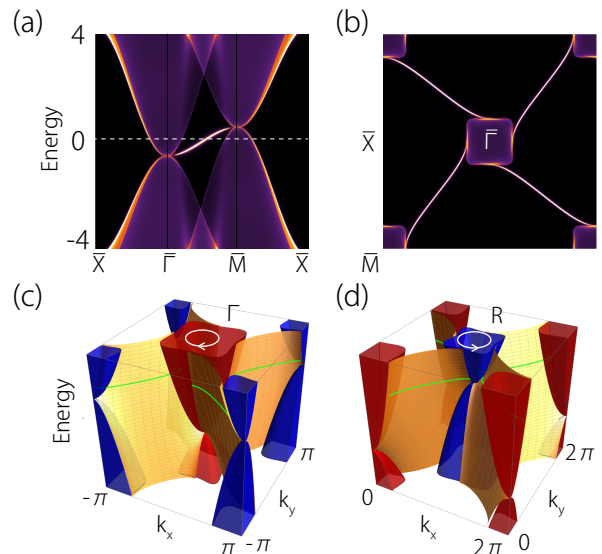


FIG. 5. Surface spectra of the lattice model in Fig. 2(c). (a) Projected spectrum on (001) surface. (b) The slice at constant energy $E_F = 0$ on (001) surface. (c-d) The quadruple helicoid surface state calculated from the lattice model (11) confined in z -direction. (c) and (d) show (001) surface bands centered at $\bar{\Gamma}$ and \bar{M} , respectively. Red and blue surfaces denote bulk band spectra, and the orange surfaces denote the four arc surface states. Green line show four Fermi arcs at a given energy.

In Fig. 5, we calculated the (001) surface state of the lattice model (11). The two C-4 WPs are projected to $\bar{\Gamma}$ and \bar{M} points of the surface BZ. Four extensive Fermi arcs connecting the $\bar{\Gamma}$ and \bar{M} points can be observed, as shown in Fig. 5(b). To further show the geometry structure of the surface state, we calculate the band structure of a slab (confined in z -direction) based on the model (11). The obtained results are plotted in Fig. 5(c) and 5(d). It indeed shows four screw surfaces, e.g. the quadruple-helicoid surface state around $\bar{\Gamma}$ and \bar{M} points. Particularly, the chirality of the helicoid reflects the chirality of the C-4 WPs. For example, by increasing energy, the four Fermi arcs clockwise wind around $\bar{\Gamma}$ point, while they anti-clockwise wind around \bar{M} point. Hence, the helicoids around $\bar{\Gamma}$ point and \bar{M} point have opposite chirality, consistent with chirality of the two C-4 WPs at Γ and R points.

IV. DISCUSSION AND CONCLUSION

Since the C-4 WP is protected by symmetry, it is interesting to study its evolution under symmetry breaking. Several interesting cases are shown in Fig. 6. Start from the lattice model (11), which has PG O and \mathcal{T} symmetry. Breaking $C_{2,110}$, the PG O descends to PG T , the two C-4 WPs at Γ and R points will persist. It again demonstrates that the PG T together with \mathcal{T} symmetry can stabilize the C-4 WP. By further breaking C_{2x} , the

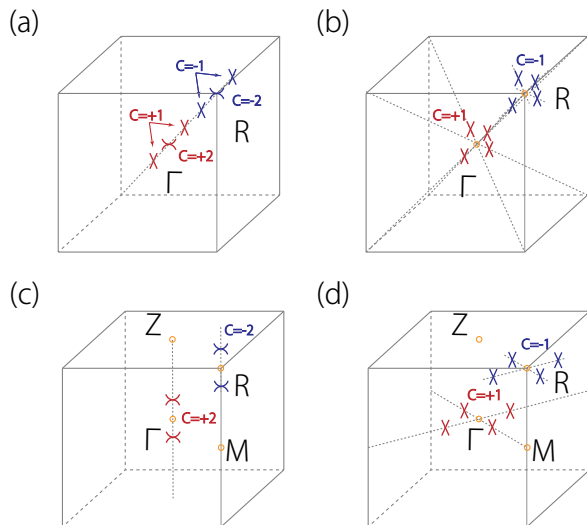


FIG. 6. C-4 WP under symmetry breaking. Start from the lattice model in Fig. 2(c). (a) breaks $C_{2,110}$ and C_{2x} symmetry, (b) breaks $C_{2,110}$ and \mathcal{T} symmetry and (c-d) only breaks $C_{3,111}^+$ symmetry.

C-4 WP at Γ (R) point would splitting into a C-2 WP locating at the original position and two C-1 WP residing on (111) axis, as shown in Fig. 6(a). If we break \mathcal{T} instead of C_{2x} , then the C-4 WP would be transformed into four C-1 WPs, which occur on the body diagonals of BZ, as shown in Fig. 6(b). Moreover, when only $C_{3,111}^+$ is broken, the C-4 WPs may split into two C-2 WPs appearing at Γ -Z (R -M) path [Fig. 6(c)] or four C-1 WPs residing at Γ -M (Z -R) path [Fig. 6(d)], depending on model parameters.

Since the C-4 WP only appears in spinless systems, it cannot be realized in real materials with sizable SOC

effect. Nevertheless, the C-4 WP may occur at phonon spectrum, as shown in Ref. [43], and the materials with negligible SOC effect. More intriguing possibility may be the artificial crystals, such as the photonic and acoustic crystals, which are spinless systems, and can be well controlled by current technology [56–59]. Hence, one can expect that the C-4 WP can be realized in these artificial systems, and the chirality-dependent properties of C-4 WP predicted here then would be readily for detection.

In conclusion, we systematically study the symmetry requirement, and the electronic, optical and magnetic properties of a newly found emergent particle, e.g. the C-4 WP. We show the minimum symmetry requirement for stabilizing a C-4 WP is $PG O$ or $PG T$ together with \mathcal{T} symmetry. We also construct a minimum lattice model for the C-4 WP. Based on both the low-energy effective model and minimum lattice model, we investigate the Landau spectrum, quantized CPGE, and quadruple-helicoid surface states of the C-4 WP, and show they all have a strong dependence on the chirality of the C-4 WP. At last, we show under symmetry breaking, the C-4 WP would be transformed into many different topological phases.

ACKNOWLEDGMENTS

The authors thank J. Xun for helpful discussions. This work is supported by the National Key R&D Program of China (Grants No. 2020YFA0308800), the NSF of China (Grants No. 12061131002, No. 12004035, and No. 11734003), the Strategic Priority Research Program of the Chinese Academy of Sciences (Grant No. XDB30000000), and the Beijing Institute of Technology Research Fund Program for Young Scholars.

-
- [1] X. Wan, A. M. Turner, A. Vishwanath, and S. Y. Savrasov, Topological semimetal and fermi-arc surface states in the electronic structure of pyrochlore iridates, *Physical Review B* **83**, 205101 (2011).
- [2] S. Murakami, Phase transition between the quantum spin hall and insulator phases in 3d: emergence of a topological gapless phase, *New Journal of Physics* **9**, 356 (2007).
- [3] C.-K. Chiu, J. C. Teo, A. P. Schnyder, and S. Ryu, Classification of topological quantum matter with symmetries, *Reviews of Modern Physics* **88**, 035005 (2016).
- [4] N. Armitage, E. Mele, and A. Vishwanath, Weyl and dirac semimetals in three-dimensional solids, *Reviews of Modern Physics* **90**, 015001 (2018).
- [5] T. Zhang, Y. Jiang, Z. Song, H. Huang, Y. He, Z. Fang, H. Weng, and C. Fang, Catalogue of topological electronic materials, *Nature* **566**, 475 (2019).
- [6] M. Vergniory, L. Elcoro, C. Felser, N. Regnault, B. A. Bernevig, and Z. Wang, A complete catalogue of high-quality topological materials, *Nature* **566**, 480 (2019).
- [7] F. Tang, H. C. Po, A. Vishwanath, and X. Wan, Comprehensive search for topological materials using symmetry indicators, *Nature* **566**, 486 (2019).
- [8] A. Burkov, Chiral anomaly and transport in weyl metals, *Journal of Physics: Condensed Matter* **27**, 113201 (2015).
- [9] Z.-M. Yu, Y. Yao, and S. A. Yang, Predicted unusual magnetoresponse in type-ii weyl semimetals, *Physical review letters* **117**, 077202 (2016).
- [10] H.-Z. Lu and S.-Q. Shen, Quantum transport in topological semimetals under magnetic fields, *Frontiers of Physics* **12**, 1 (2017).
- [11] W. Chen, H.-Z. Lu, and O. Zilberberg, Weak localization and antilocalization in nodal-line semimetals: Dimensionality and topological effects, *Physical review letters* **122**, 196603 (2019).
- [12] Y. Liu, Z.-M. Yu, C. Xiao, and S. A. Yang, Quantized circulation of anomalous shift in interface reflection, *Physical Review Letters* **125**, 076801 (2020).
- [13] C. Fang, M. J. Gilbert, X. Dai, and B. A. Bernevig, Multi-weyl topological semimetals stabilized by point group symmetry, *Physical review letters* **108**, 266802 (2012).

- (2012).
- [14] B.-J. Yang and N. Nagaosa, Classification of stable three-dimensional dirac semimetals with nontrivial topology, *Nature communications* **5**, 1 (2014).
- [15] Z. Liu, B. Zhou, Y. Zhang, Z. Wang, H. Weng, D. Prabhakaran, S.-K. Mo, Z. Shen, Z. Fang, X. Dai, *et al.*, Discovery of a three-dimensional topological dirac semimetal, *na3bi*, *Science* **343**, 864 (2014).
- [16] X. Huang, L. Zhao, Y. Long, P. Wang, D. Chen, Z. Yang, H. Liang, M. Xue, H. Weng, Z. Fang, *et al.*, Observation of the chiral-anomaly-induced negative magnetoresistance in 3d weyl semimetal *taas*, *Physical Review X* **5**, 031023 (2015).
- [17] L. Yang, Z. Liu, Y. Sun, H. Peng, H. Yang, T. Zhang, B. Zhou, Y. Zhang, Y. Guo, M. Rahn, *et al.*, Weyl semimetal phase in the non-centrosymmetric compound *taas*, *Nature physics* **11**, 728 (2015).
- [18] H. Weng, Y. Liang, Q. Xu, R. Yu, Z. Fang, X. Dai, and Y. Kawazoe, Topological node-line semimetal in three-dimensional graphene networks, *Physical Review B* **92**, 045108 (2015).
- [19] S.-Y. Xu, I. Belopolski, D. S. Sanchez, C. Zhang, G. Chang, C. Guo, G. Bian, Z. Yuan, H. Lu, T.-R. Chang, *et al.*, Experimental discovery of a topological weyl semimetal state in *tap*, *Science advances* **1**, e1501092 (2015).
- [20] B. Lv, H. Weng, B. Fu, X. P. Wang, H. Miao, J. Ma, P. Richard, X. Huang, L. Zhao, G. Chen, *et al.*, Experimental discovery of weyl semimetal *taas*, *Physical Review X* **5**, 031013 (2015).
- [21] Z. Zhu, G. W. Winkler, Q. Wu, J. Li, and A. A. Soluyanov, Triple point topological metals, *Physical Review X* **6**, 031003 (2016).
- [22] K. Deng, G. Wan, P. Deng, K. Zhang, S. Ding, E. Wang, M. Yan, H. Huang, H. Zhang, Z. Xu, *et al.*, Experimental observation of topological fermi arcs in type-ii weyl semimetal *mote 2*, *Nature Physics* **12**, 1105 (2016).
- [23] B. Bradlyn, J. Cano, Z. Wang, M. Vergniory, C. Felser, R. J. Cava, and B. A. Bernevig, Beyond dirac and weyl fermions: Unconventional quasiparticles in conventional crystals, *Science* **353** (2016).
- [24] J. Gooth, A. C. Niemann, T. Meng, A. G. Grushin, K. Landsteiner, B. Gotsmann, F. Menges, M. Schmidt, C. Shekhar, V. Süß, *et al.*, Experimental signatures of the mixed axial-gravitational anomaly in the weyl semimetal *nbp*, *Nature* **547**, 324 (2017).
- [25] W. Wu, Y. Liu, S. Li, C. Zhong, Z.-M. Yu, X.-L. Sheng, Y. Zhao, and S. A. Yang, Nodal surface semimetals: Theory and material realization, *Physical Review B* **97**, 115125 (2018).
- [26] Z.-M. Yu, W. Wu, X.-L. Sheng, Y. Zhao, and S. A. Yang, Quadratic and cubic nodal lines stabilized by crystalline symmetry, *Physical Review B* **99**, 121106 (2019).
- [27] W. Wu, Z.-M. Yu, X. Zhou, Y. Zhao, and S. A. Yang, Higher-order dirac fermions in three dimensions, *Physical Review B* **101**, 205134 (2020).
- [28] B. Lv, T. Qian, and H. Ding, Experimental perspective on three-dimensional topological semimetals, *Reviews of Modern Physics* **93**, 025002 (2021).
- [29] Z.-M. Yu, Z. Zhang, G.-B. Liu, W. Wu, X.-P. Li, R.-W. Zhang, S. A. Yang, and Y. Yao, Encyclopedia of emergent particles in three-dimensional crystals, *arXiv preprint arXiv:2102.01517* (2021).
- [30] N. Nagaosa, T. Morimoto, and Y. Tokura, Transport, magnetic and optical properties of weyl materials, *Nature Reviews Materials* **5**, 621 (2020).
- [31] G. Xu, H. Weng, Z. Wang, X. Dai, and Z. Fang, Chern semimetal and the quantized anomalous hall effect in *hgcr 2 se 4*, *Physical review letters* **107**, 186806 (2011).
- [32] S. Han, C. Lee, E.-G. Moon, and H. Min, Emergent anisotropic non-fermi liquid at a topological phase transition in three dimensions, *Physical review letters* **122**, 187601 (2019).
- [33] J.-R. Wang, G.-Z. Liu, and C.-J. Zhang, Topological quantum critical point in a triple-weyl semimetal: Non-fermi-liquid behavior and instabilities, *Physical Review B* **99**, 195119 (2019).
- [34] S.-X. Zhang, S.-K. Jian, and H. Yao, Quantum criticality preempted by nematicity, *Physical Review B* **103**, 165129 (2021).
- [35] O. Stenull, C. Kane, and T. Lubensky, Topological phonons and weyl lines in three dimensions, *Physical review letters* **117**, 068001 (2016).
- [36] K. Li, C. Li, J. Hu, Y. Li, and C. Fang, Dirac and nodal line magnons in three-dimensional antiferromagnets, *Physical review letters* **119**, 247202 (2017).
- [37] X. Zhang, M. Xiao, Y. Cheng, M.-H. Lu, and J. Christensen, Topological sound, *Communications Physics* **1**, 1 (2018).
- [38] S. Imhof, C. Berger, F. Bayer, J. Brehm, L. W. Molenkamp, T. Kiessling, F. Schindler, C. H. Lee, M. Greiter, T. Neupert, *et al.*, Topoelectrical-circuit realization of topological corner modes, *Nature Physics* **14**, 925 (2018).
- [39] B. Yang, Q. Guo, B. Tremain, R. Liu, L. E. Barr, Q. Yan, W. Gao, H. Liu, Y. Xiang, J. Chen, *et al.*, Ideal weyl points and helicoid surface states in artificial photonic crystal structures, *Science* **359**, 1013 (2018).
- [40] T. Ozawa, H. M. Price, A. Amo, N. Goldman, M. Hafezi, L. Lu, M. C. Rechtsman, D. Schuster, J. Simon, O. Zilberberg, *et al.*, Topological photonics, *Reviews of Modern Physics* **91**, 015006 (2019).
- [41] N. Cooper, J. Dalibard, and I. Spielman, Topological bands for ultracold atoms, *Reviews of modern physics* **91**, 015005 (2019).
- [42] M. Xiao, L. Ye, C. Qiu, H. He, Z. Liu, and S. Fan, Experimental demonstration of acoustic semimetal with topologically charged nodal surface, *Science advances* **6**, eaav2360 (2020).
- [43] T. Zhang, R. Takahashi, C. Fang, and S. Murakami, Twofold quadruple weyl nodes in chiral cubic crystals, *Physical Review B* **102**, 125148 (2020).
- [44] Q.-B. Liu, Y. Qian, H.-H. Fu, and Z. Wang, Symmetry-enforced weyl phonons, *npj Computational Materials* **6**, 1 (2020).
- [45] B. Bradlyn, L. Elcoro, J. Cano, M. Vergniory, Z. Wang, C. Felser, M. Aroyo, and B. A. Bernevig, Topological quantum chemistry, *Nature* **547**, 298 (2017).
- [46] J. Cano, B. Bradlyn, Z. Wang, L. Elcoro, M. G. Vergniory, C. Felser, M. I. Aroyo, and B. A. Bernevig, Building blocks of topological quantum chemistry: Elementary band representations, *Phys. Rev. B* **97**, 035139 (2018).
- [47] B. J. Wieder and C. Kane, Spin-orbit semimetals in the layer groups, *Physical Review B* **94**, 155108 (2016).
- [48] Z.-M. Yu, W. Wu, Y. Zhao, and S. A. Yang, Circumventing the no-go theorem: A single weyl point without surface fermi arcs, *Physical Review B* **100**, 041118 (2019).

- [49] D. Son and B. Spivak, Chiral anomaly and classical negative magnetoresistance of weyl metals, *Physical Review B* **88**, 104412 (2013).
- [50] J. Xiong, S. K. Kushwaha, T. Liang, J. W. Krizan, M. Hirschberger, W. Wang, R. J. Cava, and N. P. Ong, Evidence for the chiral anomaly in the dirac semimetal na3bi, *Science* **350**, 413 (2015).
- [51] Y. Zhao and S. A. Yang, Index theorem on chiral landau bands for topological fermions, *Physical Review Letters* **126**, 046401 (2021).
- [52] J. Nilsson, A. C. Neto, F. Guinea, and N. Peres, Electronic properties of bilayer and multilayer graphene, *Physical Review B* **78**, 045405 (2008).
- [53] F. de Juan, A. G. Grushin, T. Morimoto, and J. E. Moore, Quantized circular photogalvanic effect in weyl semimetals, *Nature communications* **8**, 1 (2017).
- [54] C. Fang, L. Lu, J. Liu, and L. Fu, Topological semimetals with helicoid surface states, *Nature Physics* **12**, 936 (2016).
- [55] T. Zhang, Z. Song, A. Alexandradinata, H. Weng, C. Fang, L. Lu, and Z. Fang, Double-weyl phonons in transition-metal monosilicides, *Physical review letters* **120**, 016401 (2018).
- [56] L. Lu, L. Fu, J. D. Joannopoulos, and M. Soljačić, Weyl points and line nodes in gyroid photonic crystals, *Nature photonics* **7**, 294 (2013).
- [57] W.-J. Chen, M. Xiao, and C. T. Chan, Photonic crystals possessing multiple weyl points and the experimental observation of robust surface states, *Nature communications* **7**, 1 (2016).
- [58] F. Li, X. Huang, J. Lu, J. Ma, and Z. Liu, Weyl points and fermi arcs in a chiral phononic crystal, *Nature Physics* **14**, 30 (2018).
- [59] H. He, C. Qiu, L. Ye, X. Cai, X. Fan, M. Ke, F. Zhang, and Z. Liu, Topological negative refraction of surface acoustic waves in a weyl phononic crystal, *Nature* **560**, 61 (2018).